Versatile Solution Phase Triangular Silver Nanoplates for Highly Sensitive Plasmon Resonance Sensing

Denise E. Charles,[†,*] Damian Aherne,[‡] Matthew Gara,[‡] Deirdre M. Ledwith,[§] Yurii K. Gun'ko,[‡] John M. Kelly,[‡] Werner J. Blau,[†] and Margaret E. Brennan-Fournet[§,*]

[†]School of Physics, [‡]School of Chemistry, Trinity College Dublin, Ireland and [§]School of Physics, [§]National University Ireland, Galway

ABSTRACT Solution phase triangular silver nanoplates (TSNP) with versatile tunability throughout the visible—NIR wavelengths are presented as highly sensitive localized surface plasmon refractive index sensors. A range of 20 TSNP solutions with edge lengths ranging from 11 to 200 nm and aspect ratios from 2 to 13 have been studied comprehensively using AFM, TEM, and UV—vis—NIR spectroscopy. Studies of the localized surface plasmon resonance (LSPR) peak's sensitivity to refractive index changes are performed using a simple sucrose concentration method whereby the surrounding refractive index can solely be changed without variation in any other parameter. The dependence of the TSNP localized surface plasmon resonance (LSPR) peak wavelength λ_{max} and its bulk refractive index sensitivity on the nanoplate's structure is determined. LSPR sensitivities are observed to increase linearly with λ_{max} up to 800 nm, with the values lying within the upper limit theoretically predicted for optimal sensitivity, notwithstanding any diminution due to ensemble averaging. A nonlinear increase in sensitivity is apparent at wavelengths within the NIR region with values reaching 1096 nm · RIU^{-1} at λ_{max} 1093 nm. Theoretical studies performed using a simple aspect ratio dependent approximation method and discrete dipole approximation methods confirm the dependence of the LSPR bulk refractive index sensitivity upon the TSNP aspect ratio measured experimentally. These studies highlight the importance of this key parameter in acquiring such high sensitivities and promote these TSNP sols for sensing applications at appropriate wavelengths for biological samples.

KEYWORDS: localized surface plasmon resonance (LSPR) · sensitivity · silver nanostructures · refractive index · sensor

The extraordinary optical properties of noble metal nanoparticles have led to significant interest into their potential application as subwavelength optical elements in a diverse range of technologies across all scientific fields. These optical properties are governed by their unique localized surface plasmon resonance (LSPR), that is, the collective oscillation of the nanostructure's conduction band electrons in resonance with the incident electromagnetic field.[1] The spectrum of the LSPR oscillation is strongly reliant upon the nanostructure's size,[2] shape,[3] dielectric constant,[4−7] and the dielectric constant of the surrounding environment.[8−10] The recognition of LSPR sensitivity to changes in these parameters has resulted in intense development of noble metal nanostructures for applications including molecular rulers,[11] bioimaging agents,[12] glucose concentration markers,[13] and chemical and biological sensing.[14−16] The utilization of local medium refractive index induced LSPR sensitivity *via* specific binding of analyte molecules to capture ligand-functionalized nanostructures, in particular, opens a route to ultrasensitive biosensors.

Nonspherical nanostructures (*e.g.*, nanoprisms, nanorods, or nanoshells) have been postulated to exhibit increased LSPR sensitivities *via* the support of large surface charge polarizability and increased local field enhancement, which they have been shown to display due to their sharp geometries.[17,18] High LSPR sensitivities for a variety of substrate bound, shaped, single nanostructures have been reported in the literature to date, including those for single silver nanoprisms,[19] silver nanocubes,[20] gold nanostars,[21] and gold nanoshells.[22] Sensitivity values as large as 0.79 eV · RIU^{-1} for single silver nanocubes[20] and 1.41 eV · RIU^{-1} for dielectric substrate coupled single gold nanostars[21] have been recorded. Significantly increased LSPR sensitivities have been measured for more complex coupled plasmonic nanostructures such as 801 nm · RIU^{-1} for hematite core/Au shell nanorice at a LSPR peak wavelength λ_{max} of 1160 nm[23] and 880 nm · RIU^{-1} for gold nanorings at a λ_{max} of 1545 nm.[24] As seen from these reported sensitivities, an inconsistency exists in the units used to express the linear refractive index sensitivity of the varying nanostructures, with some authors quoting eV · RIU^{-1} and others nm · RIU^{-1}. Due to this inconsistency, Sherry *et al.*[20] defined a figure of merit (FOM) as a way of defining the overall sensitive response of a plasmonic nanostructure, where the FOM can be expressed as the ratio

*Address correspondence to charled@tcd.ie, margaret.brennanfournet@nuigalway.ie.

Received for review June 17, 2009 and accepted December 15, 2009.

Published online December 23, 2009. 10.1021/nn9016235

between the linear refractive index sensitivity of the nanostructure divided by its LSPR full width at half-maximum (fwhm). Unger *et al.*[25] also recently defined an analytical expression for the FOM of a nanostructure's sensitivity based on a more statistical analysis. The FOM expression defined by Sherry *et al.* is used in this study as it is more universally quoted.

The majority of LSPR sensitivity values reported to date are for single nanostructures bound to a dielectric substrate. Coupling to a substrate can influence the sensitivity of isolated nanostructures to refractive index change either enhancing it[10] or diminishing it,[26] depending on the dielectric properties of the substrate and the orientation of the nanostructure on the substrate, compared to that observed for the nanostructure in solution. Limited research has been undertaken to examine solution phase LSPR sensing despite it having the obvious advantage of the nanostructure sensor being homogeneously in phase with the biological target molecule. Nevertheless, the solution phase nanostructures that have been presented in literature to date have displayed promising bulk refractive index sensitivities,[27−30] encouraging further analysis into their biosensing capabilities. It is important to note, however, that the application of nanostructures in biosensing applications is limited by the position of water and biomolecular absorption wavelengths. This signifies that the nanostructures LSPR λ_{max} should be preferentially removed from these absorption wavelengths, thus highlighting that nanostructures with tunable LSPR wavelengths are optimal in such applications.

Solution phase triangular silver nanoplates (TSNP) are herein examined as tunable LSPR sensors with excellent potential for versatile and highly responsive biosensing. Such highly anisotropic silver nanoplates have received considerable interest due the ability to tune their in-plane dipole LSPR across the visible spectrum and into the NIR.[31] It is postulated that silver nanoparticles are advantageous over other noble metal nanoparticles within visible wavelengths as their LSPR energy is removed from interband transitions (3.8 eV $\sim$ 327 nm).[32] This results in a narrow LSPR fwhm which exhibits a much stronger shift with increasing local dielectric constant than is the case of gold or copper at these wavelengths.[32,33] At wavelengths within the NIR region, these interband transitions do not influence the plasmon resonance of noble metals. Previous studies have shown that gold nanoparticles are more biologically compatible than silver due to the high oxidation rate of silver and chemical stability of gold nanoparticles. However, recent advances have been made in functionalizing and altering the surface chemistry of silver nanostructures such as these TSNP,[34] stabilizing them under physiological conditions, thus enabling exploitation of their high sensitivities in biological applications.

Previously, we reported the synthesis of such TSNP sols of high geometric uniformity for which the edge length can be readily controlled, enabling the systematic tuning of the LSPR throughout the visible and NIR spectrum.[35] The TSNP sols are prepared using a seed mediated approach involving the reduction of silver ions by ascorbic acid that produces over 95% nanoplate populations in a rapid reproducible manner. The narrow geometric distribution of the TSNP within the sol leads to a highly uniform response of the ensemble upon interaction with an electromagnetic field. Unlike our previous solution phase silver nanoplates,[36,37] these sols do not require the presence of a stabilizing polymer during fabrication, which leads to easier sample preparation for sensitivity analysis. Through analyzing the sensitivity of TSNP sols with varying edge lengths, we can gain an understanding of the potential these nanostructures hold for biosensing applications. In addition, we can compare this potential with that reported for other noble metal nanostructures in literature and obtain insight into the essential features required by a nanostructure for highly efficient biosensing applications.

RESULTS AND DISCUSSION

TSNP sols were prepared using the method previously described, with their size systematically changed by the adjustment of the volume of seeds in the nanoplate growth mixture.[35] A series of 20 TSNP sols with increasing edge length from 11 to 197 nm were prepared. AFM and TEM images (Figure 1) were recorded and analyzed to assess the influence of the nanostructures' geometry upon the position of the LSPR. Due to the thinness of the nanoplate, compared to its long edge length (Figure 1c), shade variations are apparent in the TEM image shown. Similar variations in shade have been observed in TEM images of silver and gold nanoplate structures,[38,39] which are attributed to bending induced variation in the metal's atomic plane due to the thinness of the nanostructure.[40] Using a statistically satisfactory number of nanoplates (approximately 150−200 nanoplates) for each of the 20 ensembles, the mean thickness (nm) and the mean edge length (nm) were calculated. The AFM measurements show a slight increase in the mean thickness of the TSNP ensembles with increasing edge length recorded *via* TEM (Figure 2a). (Previously, it was reported that these TSNP did not display a change in thickness with varying edge length;[35] however, this study was based on a smaller range of edge lengths.) Due to this gradual increase in thickness of the TSNP with increasing edge length, we believe that the dependence of the LSPR λ_{max} on such a nanostructure is better examined using the nanoplate aspect ratio *R*, where *R* is the TSNP edge length divided by the thickness of the nanoplate. The aspect ratio of the TSNP is found to increase from values of 2 to 13 with edge lengths ranging from 11 to 197 nm (Figure 2B).

LSPR extinction spectra of a number of the 20 TSNP sols tested are shown in Figure 3a, displaying the strong

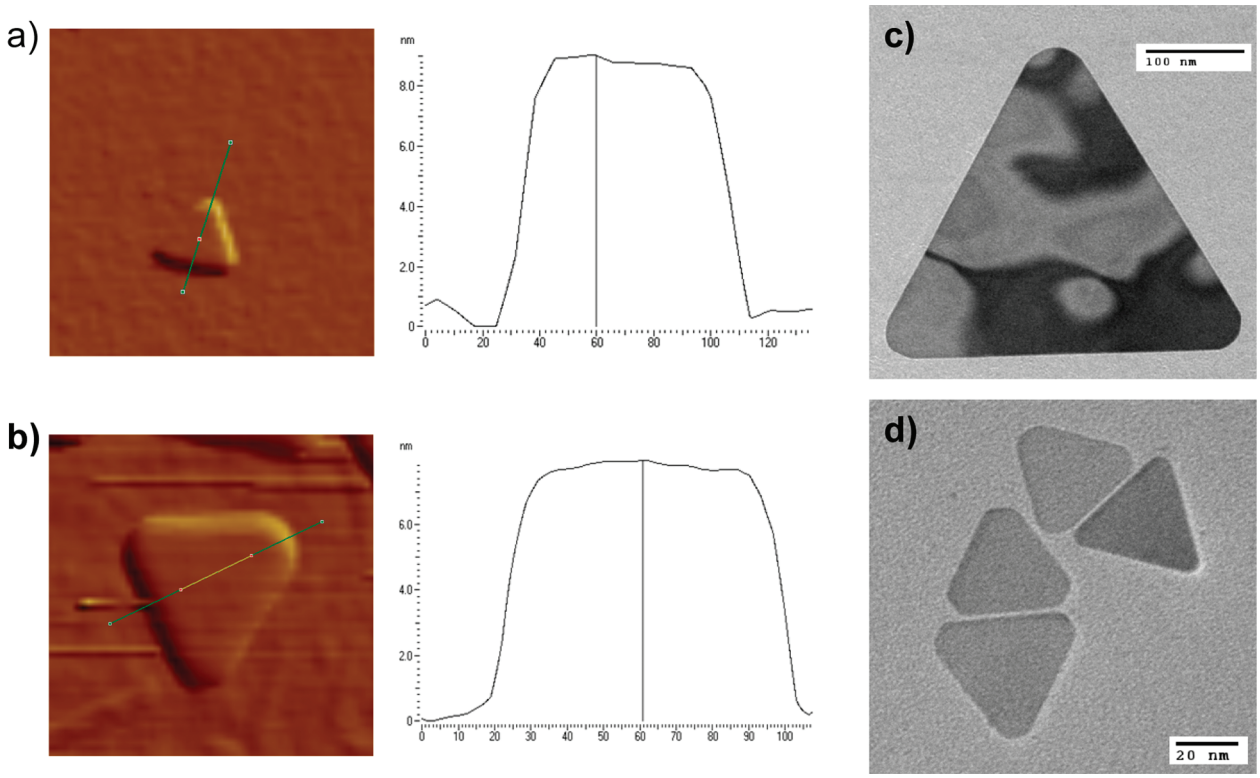

Figure 1. (a) AFM image and height profile of a typical TSNP of thickness 9 nm and (b) AFM image and profile of TSNP of thickness 8 nm. (c,d) TEM images showing some of the various sized samples fabricated. Such images were used to measure the diagonal and edge length of the triangular face of the nanoplates.

dominant dipolar resonance of these high aspect ratio nanostructures. The ensembles' LSPR λ_{max} is observed to red shift as the aspect ratio increases for LSPR within the range of 500−1150 nm (Figure 3b).

To assess the potential use of the TSNP samples for various refractive index based sensing applications, it is important to determine how the λ_{max} varies with the refractive index surrounding the nanoplate. This has previously been tested in some cases using various solvents. However, with some solvents, it has been reported that changes in the geometry of the nanostructure upon exposure to the solvents used may occur,[41,42] or pretreatment of the nanostructure before analysis to prevent such a change occurring may be required.[10] In our study, we have adopted a simple sucrose method whereby the bulk refractive index of the solution surrounding the TSNP was changed through a variation in sucrose concentration. With this method, it must be noted that the refractive index near the surface may differ from that of the bulk. While it is possible that the sucrose might bind preferentially to the surface, this would be expected to lead to a nonlinear response to changes in the sucrose concentration, which is not observed in the case of these TSNP sols (Supporting Information). Therefore, this bulk refractive index method and similar approaches[27,28] are valuable methods of indicating how efficiently such plasmonic nanostructures would perform as biosensors.

Figure 4a shows an example of the spectral shift observed for a 82 nm edge length TSNP ensemble sus-

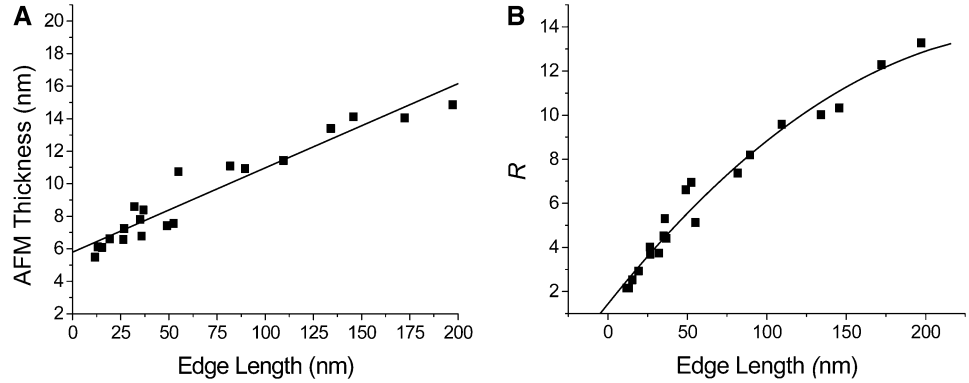

Figure 2. (A) Linear fit to the structural data depicting the relationship between the nanoplate ensembles' mean edge length (nm) and mean thickness (nm). (B) Increase in the TSNP aspect ratio with increasing edge length.

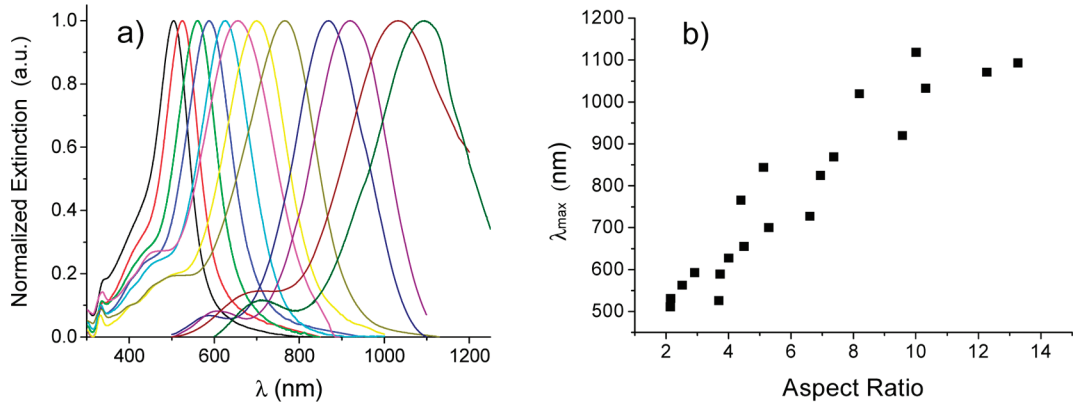

Figure 3. (a) Tunability of the LSPR λ_{max} of the TSNP sols within the visible and NIR. (b) Plot depicting the dependence of the ensembles' peak wavelength on the mean aspect ratio measured for the various samples.

pended in the various concentrations of sucrose used. TSNP sensitivities are found to increase linearly with LSPR λ_{max}; however, a dramatic increase in sensitivity occurs at the longer wavelengths with values reaching a maximum of 1096 nm · RIU^{-1} at a λ_{max} of 1093 nm for TSNP with an aspect ratio of 13 (Figure 4b). By reviewing previous LSPR sensitivities presented in literature for various LSPR nanostructures, it is evident that the highest sensitivities of the TSNP sols examined here are greater than those recorded to date, including those for single nanostructures such as nanorice,[23] gold nanorings,[24] and gold nanostars (see Table 1 in Supporting Information).[21] Furthermore, unlike other reported high LSPR sensitive nanostructures, the high TSNP sensitivities occur at wavelengths shorter than 1150 nm, before water and biomolecular absorptions can become limiting factors in their suitability as biosensors. In addition to this, the TSNP ensemble sensitivity values of 290−433 nm · RIU^{-1} for sols with LSPR peak wavelengths in the visible exceed those previously reported for nanostructures within this wavelength band such as 205 nm · RIU^{-1} for single Au triangles by Sherry *et al.*[19] with LSPR λ_{max} at 631 nm and 285 nm · RIU^{-1} for Au nanorattles in solution with a λ_{max} of approximately 650 nm.[29]

The FOM as defined by Sherry *et al.*[20] is the most commonly used in literature for defining nanostructures' sensitivities; therefore, it is used here to enable further comparison of the TSNP sols' sensitivities with those previously reported. The fwhm values of the TSNP sols spectra are observed to vary from 100 up to 285 nm with corresponding red shift in the LSPR λ_{max} (Figure 5a), resulting in FOM values ranging from 1.8 up to 4.3 (Figure 5b). These FOM values are comparable to those previously recorded for more complex structures, such as solution phase gold nanobipyramids with a FOM of 4.5 at a λ_{max} 1090 nm.[28] Indeed, the FOM for the TSNP sols presented here would be among the highest reported to date if it were not for reductions in the FOM values due to broader line widths at higher wavelengths (Table 1 Supporting Information). It may, of course, be noted that the FOM for larger particles require measurements within the near-IR which may make practical implementation more complicated.

From Figures 4a and b, it is apparent that the enhanced sensitivities recorded for the TSNP sols display a distinct dependence upon the spectral position of the LSPR λ_{max}. The spectral dependence observed agrees with the model predicted by Miller *et al.*,[43] who state that the upper bound sensitivity of a nanostructure is

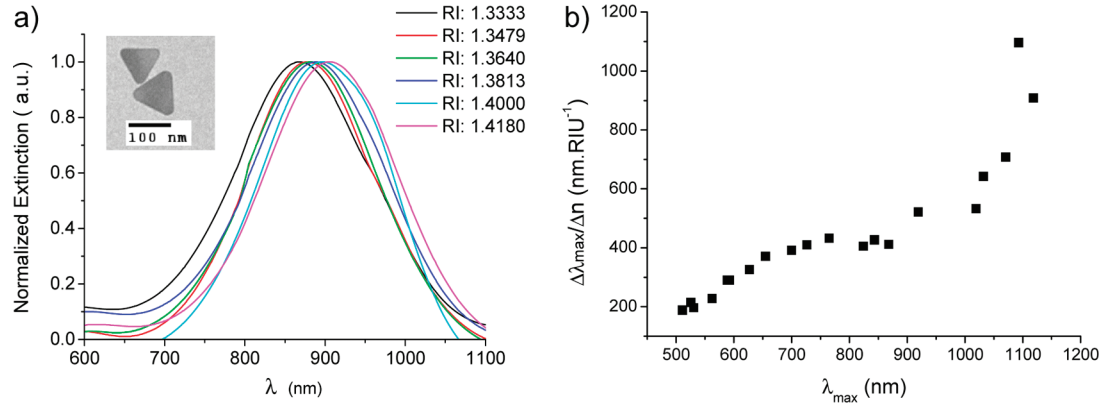

Figure 4. (a) Example of spectral shift observed for a specific TSNP ensemble with original peak wavelength of 868 nm, mean edge length 82 nm, mean thickness 11 nm, in varying sucrose concentrations. (b) Peak LSPR wavelength of the 20 samples plotted against the corresponding LSPR sensitivity of the ensemble to the sucrose refractive index analysis.

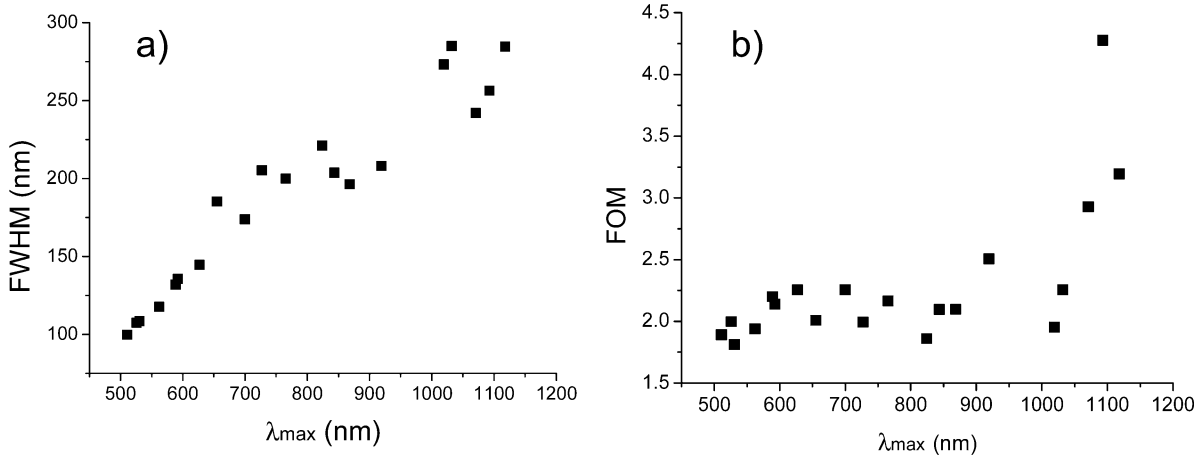

Figure 5. (a) Fwhm of the TSNP sols spectra showing an increase with red-shifted LSPR λ_{max} up to the NIR. (b) FOM of the TSNP sols as calculated by the method proposed by Sherry *et al.*

dependent solely upon its LSPR λ_{max} regardless of its structural parameters. This model does not hold for nanostructures with LSPR λ_{max} above 800 nm. Another similar theory proposed by Svedendahl *et al.* indicates that the bulk refractive index sensitivity is determined by the wavelength dependent dielectric function of the metallic nanostructure and the refractive index surrounding the nanostructure.[44] This dielectric function theory was found to hold for LSPR studies on a thin gold film and LSPR studies on an array of gold nanodisks with LSPR λ_{max} at approximately 700 nm. Other studies, however, suggest that the structural parameters of the nanostructure will contribute to determining its sensitivity. For example, silver rhombic nanostructures[45] with aspect ratios of 2.9 have been predicted by discrete dipole approximation (DDA) to have sensitivities of 330 nm · RIU^{-1}, while triangular silver nanoparticles with aspect ratios of 2 have been shown to have a value of 191 nm · RIU^{-1}.[42] Both of these earlier reported sensitivity values are in agreement with the values for the TSNP at similar aspect ratios shown in Figure 6a, signifying that there exists a potential influence of aspect ratio on LSPR sensitivity.

Aspect Ratio Dependent Approximation and DDA. In order to further assess the importance of the aspect ratio of a nanostructure in determining the LSPR sensitivity to refractive index changes, an approximation method based on the quasistatic theory developed by Miller *et al.* and discrete dipole approximation calculations are applied. Miller's quasistatic theory is based on Mie theory,[46] which states that the extinction of a metallic sphere, that is, the sum of the absorption and Rayleigh scattering can be represented by the equation

$$E = \frac{24\pi^2 N_A a^3 \varepsilon_m^{3/2}}{\lambda \ln(10)}\left[\frac{\varepsilon_i}{(\varepsilon_r + \chi\varepsilon_m)^2 + \varepsilon_i^2}\right] \quad (1)$$

where N_A is the areal density of nanoparticles, a is the radius of the metallic nanospheres, ε_m is the dielectric constant of the medium surrounding the metallic nanospheres, λ is the wavelength of the absorbing radiation, χ the nanostructure's shape factor, and ε_i and ε_r the imaginary and real parts of the nanostructure's dielectric function, respectively. The dipolar plasmon resonance condition for silver nanoparticles (eq 1), that is, the occurrence of the LSPR maximum peak, is satisfied when

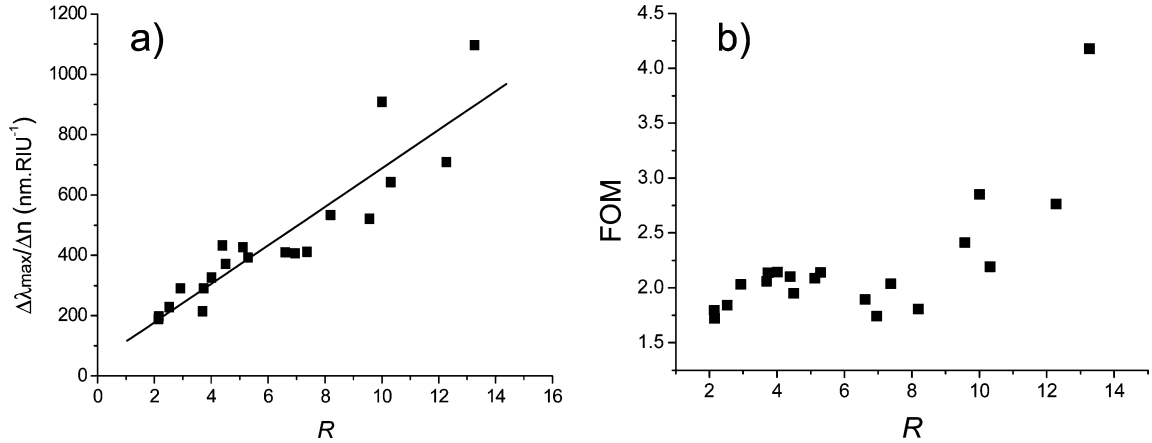

Figure 6. Dependence of (a) the LSPR linear refractive index sensitivity and (b) the FOM upon the aspect ratio of the TSNP.

$$\varepsilon_r = \chi n^2 \quad (2)$$

where n is the refractive index of the surrounding medium. From these conditions, Miller developed an approximate analytical expression given in eq 3 for the sensitivity $\Delta\lambda_{max}/\Delta n$ of the resonance wavelength to the refractive index of the medium

$$\frac{\Delta\lambda_{max}}{\Delta n} = \frac{\frac{\Delta\varepsilon_r}{\Delta n}}{\left(\frac{\Delta\varepsilon_r}{\Delta\lambda}\right)_{\lambda_{max}}} \quad (3)$$

where ε_r is the real dielectric constant of silver, $\Delta\varepsilon_r/\Delta n$ the refractive index dependence of the real dielectric constant determined by the plasmon resonance condition and $(\Delta\varepsilon_r/\Delta\lambda)_{\lambda_{max}}$ is the slope of the real part of the nanoparticle's dielectric function with changing wavelength. Due to the wavelength dependence of ε_r and the dependence of the resonance condition upon both this parameter and the shape factor χ of the nanoplates, both parameters in eq 3 will therefore define the wavelength of the LSPR maximum and hence the LSPR sensitivity of the nanoplates.

In order to determine $(\Delta\varepsilon_r/\Delta\lambda)_{\lambda_{max}}$, the real dielectric constant for silver at the various LSPR λ_{max} wavelengths measured for the TSNP was calculated using the Palik optical constants n (real refractive index) and k (extinction coefficient) for silver[47] (see Appendix 1 Supporting Information). The refractive index dependence of the real dielectric constant can be determined by the plasmon resonance condition using an oblate ellipsoidal approximation to calculate the shape factor χ (see Supporting Information).[48] Previous shape factor values of 2 for a sphere and greater than 17 for a 5:1 aspect ratio nanorod with prolate spheroid geometry have been reported.[49] The shape factor for the TSNP is found to be directly proportional to the aspect ratio and reaches a maximum of approximately 20 for the highest aspect ratios. Solving eq 3 for our water based TSNP ensembles with an ellipsoidal shape factor approximation, we find that the bulk linear refractive index sensitivity can be expressed as

$$\frac{\Delta\lambda_{max}}{\Delta n} \approx 47.85 \times \chi \quad (4)$$

Equation 4 shows that the sensitivity is linearly dependent upon the shape factor χ, which is determined by the aspect ratio R (Figure 7a). Using this relationship, sensitivity values can be computed for nanoplates with structural parameters equivalent to those determined from the AFM and TEM analysis previously described (Figure 7b). Our shape factor calculations are in agreement with the theory calculated by Miller *et al.* for wavelengths within the 500 to 800 nm region; however, they further accurately predict the LSPR sensitivities measured experimentally at longer wavelengths in the NIR. This agreement between experimental results and theoretical considerations emphasizes the importance of the aspect ratio and hence shape factor of a nanostructure in determining its LSPR sensitivity to refractive index changes.

As the oblate ellipsoidal approximation presented above does not take into account tip enhancement effects of the triangular geometry, discrete dipole approximations were also performed on a number of triangular nanoplates with aspect ratios equivalent to some of those measured in the experimental studies. The discrete dipole approximation (DDA) is a numerical method of solving Maxwell's equations for a single nanoparticle of arbitrary shape, generating its extinction, scattering, and absorption cross sections.[50] The exact shape of the nanostructure is considered by replacing the full nanoparticle structure by an array of cubic dipoles, and the optical response of the collection of dipoles to an interacting electromagnetic field is then determined. As the DDA method considers the exact shape of the TSNP, these studies can be used to establish whether the aspect ratio dependent approximation we have presented above is a true representation of the refractive index sensitivity of triangular nanoplate structures.

The DDA calculated extinction spectra for single TSNP of chosen aspect ratios are shown in Figure 8a. As the aspect ratio of the TSNP is increased, the LSPR λ_{max} was found to red shift, in agreement with the experimental results. The DDA spectra were calculated for single nanoplates rather than ensembles, resulting in discrepancies between the positions of the experimentally measured LSPR λ_{max} and those calculated using the DDA method. Differences between ensemble extinction spectra and single nanoparticle behavior have been previously reported, with some reports of a blue shift in the ensemble spectrum,[20] and others reporting a blue shift or a red shift depending on the particular single nanoparticle considered.[19,21] A red shift in the experimentally measured extinction spectrum of a periodic array of silver nanoparticles compared to their DDA predicted spectra was demonstrated by Jensen *et al.*,[9] with an increase in red shift recorded for increasing nanoparticle volume and aspect ratio.

For some of the smaller aspect ratio nanoplates, a blue shift in the experimental extinction spectra was observed when compared to their DDA calculated spectra (Figure 8b). Truncation effects have been reported to be associated with a blue shift in the LSPR λ_{max}.[17,30,51] The degree of truncation of the TSNP sols was calculated from their TEM images, where the degree of truncation is defined in eq 5.

$$\text{degree of truncation} = \frac{\text{area of truncated triangle}}{\text{area of untruncated triangle}} \times 100 \quad (5)$$

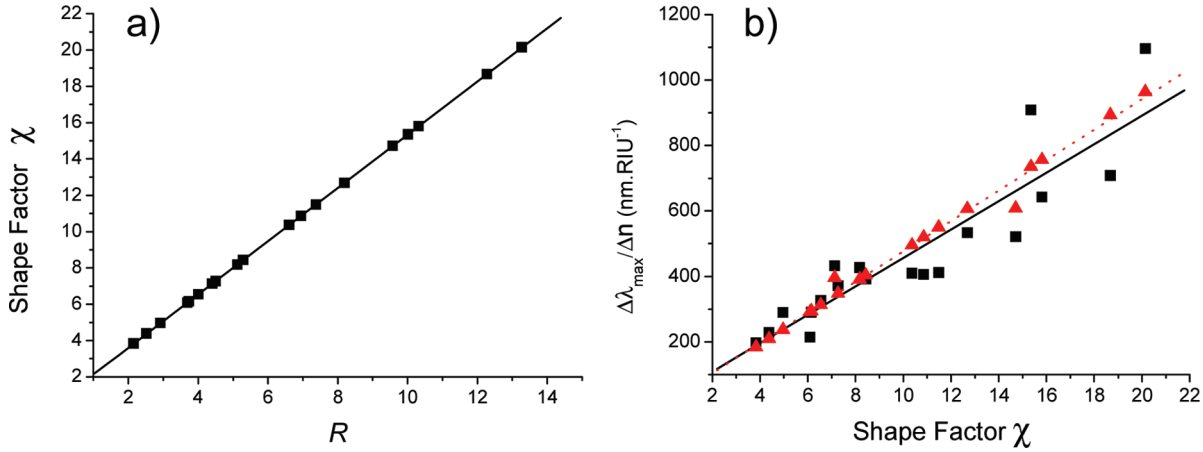

Figure 7. (a) Linear relationship between shape factor and aspect ratio. (b) Experimental sensitivities (black squares) and approximated sensitivities (red triangles) plotted against the shape factor determined through AFM and TEM studies. Linear fits through the experimental (black straight line) and the approximated sensitivities (red dotted line) show the agreement between the experimental and theoretical values.

Analysis of the degree of truncation shows that those TSNP which show a blue shift in their experimental LSPR λ_{max} compared to the DDA calculated spectra have degrees of truncation of approximately 15%, whereas TSNP which show red shifts in their experimental LSPR λ_{max} compared to the DDA calculated spectra have lesser degrees of truncation of approximately 5%. Figure 8c shows an example of a TSNP sol which showed a red shift in its experimental ensemble extinction compared to the DDA extinction of a single nanoplate of the same aspect ratio.

In order to examine the linear refractive index sensitivity of the TSNP using DDA, extinction spectra were computed for the TSNP of various aspect ratios shown in Figure 8a. The shift in the LSPR λ_{max} was calculated for the TSNP in different sucrose concentrations, and the linear refractive index sensitivity was computed using the same method as in the experimental analysis. Figure 9a shows the trend observed for the DDA calculated sensitivities as the LSPR λ_{max} is red shifted with increasing aspect ratio. Although the experimental LSPR λ_{max} for the TSNP with higher aspect ratios are red shifted with respect to the DDA results, the DDA calculated linear refractive sensitivities show a similar trend to those measured experimentally and also those predicted *via* the aspect ratio dependent approximation method. The DDA measurements therefore confirm the importance of the aspect ratio in defining the TSNP sensitive response to bulk refractive index changes, thus supporting the conclusions drawn from the aspect ratio dependent approximation method (eq 4).

In conclusion, this work presents the first detailed study of the dependence of the LSPR sensitivity of solution phase, tunable, plasmonic nanostructures with LSPR maxima over such a broad wavelength range upon their structural parameters. LSPR bulk refractive index sensitivities were observed to increase linearly up to a LSPR maximum of 800 nm with a nonlinear enhancement observed in the NIR wavelength region, reaching a maximum value of 1096 nm · RIU^{-1} at a LSPR λ_{max} at 1093 nm. The recorded sensitivities are found to exceed many of those previously reported for other nanostructures in the literature with little diminution due to

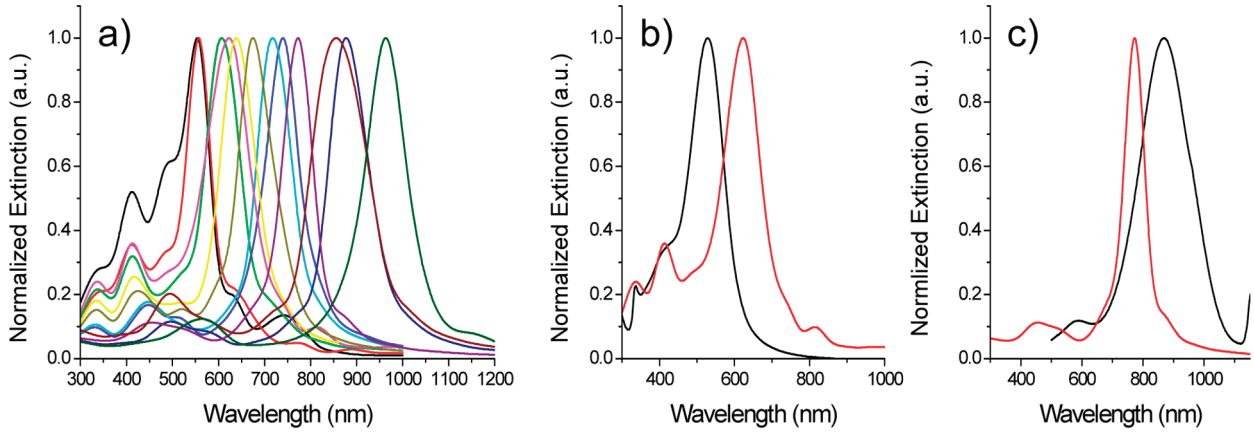

Figure 8. (a) DDA calculated spectra for TSNP of various aspect ratios. The LSPR λ_{max} was found to red shift with increasing aspect ratio, in agreement with experimental results. Comparison between experimental spectra (black) and DDA spectra (red) for (b) a TSNP sol with a mean truncation factor of approximately 15% and (c) a TSNP sol with a mean truncation factor of 5%.

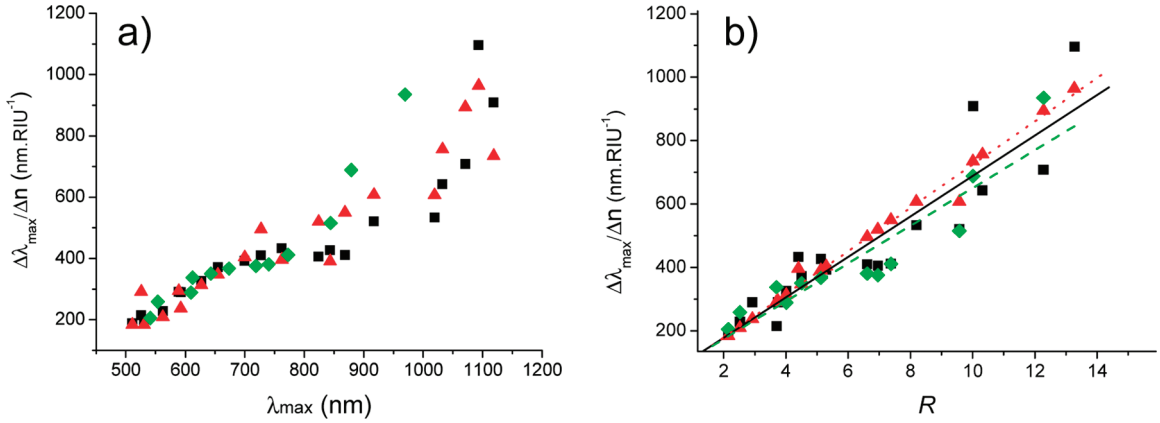

Figure 9. (a) Comparison between the bulk linear refractive index sensitivity values determined *via* experiment (black squares), using the aspect ratio dependent approximation method (red triangles) and discrete dipole approximation calculations (green diamonds). (b) Dependence of the linear refractive index sensitivity upon aspect ratio showing linear fits for all three methods (experimental fit = black straight line, approximation method = red dotted line, DDA= green dashed line).

ensemble averaging observed. LSPR sensitivity calculations based on the aspect ratio of the TSNP confirm the importance of the parameter in determining the degree of sensitivity observed, while DDA calculations have in conjunction strengthened the validity of such an approach. These results suggest that the TSNP ensembles will potentially, in turn, have high local refractive index sensitivities and act as efficient devices for biosensing applications, as they encompass aspect ratios large enough to provide high LSPR sensitivity yet low enough that the LSPR λ_{max} remains within the spectral range appropriate for biosensing. We believe that this represents a promising step toward realizing optimal nanostructures for versatile biosensing.

MATERIALS AND METHODS

TSNP Sol Preparation: TSNP sols were prepared using a silver seed-catalyzed reduction of Ag^+ as previously described.[35] The nanoplates are produced by combining 5 mL of distilled water, aqueous ascorbic acid (75 mL, 10 mM), and various quantities of seed solution, followed by addition of aqueous $AgNO_3$ (3 mL, 0.5 mM) at a rate of 1 mL min^{-1}. LSPR λ_{max} values were red shifted from the visible to NIR wavelengths by varying the volumes of seed solutions from 500 μL (λ_{max}= 500 nm) down to 2.3 μL (λ_{max}= 1090 nm). A reduction in the volume of seeds used in the preparation method results in a red shift in the LSPR λ_{max}. A series of 20 TSNP with increasing edge length from 11 to 197 nm were thus prepared.

Structural Characterization: AFM measurements were performed in tapping mode using a Multimode Nanoscope IIIA and a Si tip with a radius of approximately 10 nm. Samples were prepared on polished silicon substrates, which were first cleaned using a 5:1:1 piranha solution and then functionalized with 3-aminopropyltriethoxysilane. These functionalized substrates were then left in the nanoplate solutions for a few hours for the nanoplates to attach to the substrates. All TEM images were taken on a Jeol 2100. Both AFM images and TEM images were taken from different randomly selected areas of the sample. Using a statistically satisfactory number of nanoplates (approx 150−200 nanoplates) for each of the 20 ensembles, the mean thickness (nm) and the mean edge length (nm) were calculated with the standard deviation of the distributions representing the experimental error.

LSPR Sensitivity Analysis: Water/sucrose solutions were used to vary the refractive index of the solution within which the nanoplates were suspended. Sucrose concentrations were varied in steps of 10% from 10 up to 50 wt %. The refractive indices of the sucrose concentrations used were measured after preparation on a temperature controlled refractometer with a 589 nm LED light source. A low volume of the TSNP sol (20 μL) was then mixed in with the sucrose solutions (780 μL). The refractive index of the solution mixture surrounding the nanoplates was then calculated using the Lorentz−Lorentz equation[28]

$$\frac{n_{12}^2 - 1}{n_{12}^2 + 2} = \varphi_1 \frac{n_1^2 - 1}{n_1^2 + 2} + \varphi \frac{n_2^2 - 1}{n_2^2 + 2} \quad (6)$$

The solution phase ensemble extinction spectra of the TSNP sols suspended in the different sucrose solutions were acquired using a Cary Varian 6000i UV−vis−NIR spectrometer with the peak LSPR resonances ranging from wavelengths of about 500 up to 1090 nm. The sensitivity of the solution phase TSNP $\Delta\lambda_{max}$ RIU^{-1} can be represented by plotting the shift observed in the peak LSPR wavelength $\Delta\lambda_{max}$ against the corresponding refractive index of the sucrose. This can also be represented in energy terms as eV · RIU^{-1} for comparative analysis.

Discrete Dipole Approximation: Using the Draine and Flatau code,[50] extinction spectra were calculated for 12 nanoplate shapes suspended in four different mediums, with four different dielectric constants (48 calculations in total). The four mediums approximate as water, 10% sucrose in water, 30% sucrose in water, and 50% sucrose in water. All four dielectric constants were assumed to be noncomplex and were worked into the calculation using the relationship

$$\varepsilon = \frac{\varepsilon_{target}}{\varepsilon_{medium}} \quad (7)$$

where ε_{target} is the complex dielectric constant of silver in a vacuum.[45] The 12 shapes used for the DDA calculation were based upon the samples in the experimental data, consisting of regular triangular prisms, made up of a simple cubic array of dipoles spaced ~1 nm apart, as per the DDA method. As previously stated before, the shapes used were based upon experimental samples, but the regular triangular prism is an approximation of this; therefore, the key factors used to calculate the DDA spectra were the aspect ratio and the volume of the nanoplates measured for the nanoplates in the experimental studies.

Acknowledgment. This work was supported by Enterprise Ireland CFTD Grant 2006 114, Science Foundation Ireland Grant 06/

CHP36, and IRCSET postdoctoral fellowship (to D.A.). We thank Neal Leady and Clodagh Dooley in the Centre of Microscopy and Analysis (CMA), TCD for their assistance with the electron microscope. Financial support for transmission electron microscopy was provided by CMA's postgraduate student bursary award. We would also like to acknowledge B. Draine and P. Flatau for use of their DDA code, DDSCAT 7.0 and the Trinity Centre for High Performance Computing (TCHPC) for the use of their IITAC supercomputer.

Supporting Information Available: Figure showing the linear shift in the plasmon resonance position of the TSNP with increasing refractive index (*i.e.*, increasing concentrations of sucrose). Table comparing the TSNP sols sensitivity values with examples of those reported in literature for other plasmonic nanostructures. Theory detailing the aspect ratio dependent approximation. This material is available free of charge *via* the Internet at http://pubs.acs.org.

REFERENCES AND NOTES

1. Willets, K. A.; Van Duyne, R. P. Localized Surface Plasmon Resonance Spectroscopy and Sensing. *Annu. Rev. Phys. Chem.* **2007**, *58*, 267–297.
2. Jensen, T. R.; Malinsky, M. D.; Haynes, C. L.; Van Duyne, R. P. Nanosphere Lithography: Tunable Localized Surface Plasmon Resonance Spectra of Silver Nanoparticles. *J. Phys. Chem. B* **2000**, *104*, 10549–10556.
3. Ledwith, D. M.; Whelan, A. M.; Kelly, J. M. A Rapid, Straightforward Method for Controlling the Morphology of Stable Silver Nanoparticles. *J. Mater. Chem.* **2007**, *17*, 2459–2464.
4. Johnson, R. C.; Li, J.; Hupp, J. T.; Schatz, G. C. Hyper-Rayleigh Scattering Studies of Silver, Copper, and Platinum Nanoparticle Suspensions. *Chem. Phys. Lett.* **2002**, *356*, 534–540.
5. Chan, G. H.; Zhao, J.; Hicks, E. M.; Schatz, G. C.; Van Duyne, R. P. Plasmonic Properties of Copper Nanoparticles by Nanosphere Lithography. *Nano Lett.* **2007**, *7*, 1947–1952.
6. Doremus, R. H.; Rao, P. Optical Properties of Nanosized Gold Particles. *J. Mater. Res.* **1996**, *11*, 2834–2840.
7. Zhang, X. Y.; Hicks, E. M.; Zhao, J.; Schatz, G. C.; Van Duyne, R. P. Electrochemical Tuning of Silver Nanoparticles Fabricated by Nanosphere Lithography. *Nano Lett.* **2005**, *5*, 1503–1507.
8. Mock, J. J.; Smith, D. R.; Schultz, S. Local Refractive Index Dependence of Plasmon Resonance Spectra from Individual Nanoparticles. *Nano Lett.* **2003**, *3*, 485–491.
9. Jensen, T. R.; Duval, M. L.; Kelly, K. L.; Lazarides, A. A.; Schatz, G. C.; Van Duyne, R. P. Nanosphere Lithography: Effect of the External Dielectric Medium on the Surface Plasmon Resonance Spectrum of a Periodic Array of Silver Nanoparticles. *J. Phys. Chem. B* **1999**, *103*, 9846–9853.
10. Malinsky, M. D.; Kelly, K. L.; Schatz, G. C.; Van Duyne, R. P. Nanosphere Lithography: Effect of Substrate on the Localized Surface Plasmon Resonance Spectrum of Silver Nanoparticles. *J. Phys. Chem. B* **2001**, *105*, 2343–2350.
11. Sonnichsen, C.; Reinhard, B. M.; Liphardt, J.; Alivisatos, A. P. A Molecular Ruler Based on Plasmon Coupling of Single Gold and Silver Nanoparticles. *Nat. Biotechnol.* **2005**, *23*, 741–745.
12. Sharma, P.; Brown, S.; Walter, G.; Santra, S.; Moudgil, B. Nanoparticles for Bioimaging. *Adv. Colloid Interface Sci.* **2006**, 123−126 and 471−485.
13. Serra, A.; Filippo, E.; Re, M.; Palmisano, M.; Vittori-Antisari, M.; Buccolieri, A.; Manno, D. Non-functionalized Silver Nanoparticles for a Localized Surface Plasmon Resonance-Based Glucose Sensor. *Nanotechnology* **2009**, *20*, 165501.
14. Wang, C. Y.; Cimalla, V.; Kups, T.; Rohlig, C. C.; Stauden, T.; Ambacher, O.; Kunzer, M.; Passow, T.; Schirmacher, W.; Pletschen, W.; Kohler, K.; Wagner, J. Integration of In_2O_3 Nanoparticle Based Ozone Sensors with GaInNGaN Light Emitting Diodes. *Appl. Phys. Lett.* **2007**, *91*, 103509.
15. Zhao, J.; Zhang, X. Y.; Yonzon, C. R.; Haes, A. J.; Van Duyne, R. P. Localized Surface Plasmon Resonance Biosensors. *Nanomedicine* **2006**, *1*, 219–228.
16. Haes, A. J.; Van Duyne, R. P. A Nanoscale Optical Biosensor: Sensitivity and Selectivity of an Approach Based on the Localized Surface Plasmon Resonance Spectroscopy of Triangular Silver Nanoparticles. *J. Am. Chem. Soc.* **2002**, *124*, 10596–10604.
17. Kelly, K. L.; Coronado, E.; Zhao, L. L.; Schatz, G. C. The Optical Properties of Metal Nanoparticles: The Influence of Size, Shape, and Dielectric Environment. *J. Phys. Chem. B* **2003**, *107*, 668–677.
18. Haes, A. J.; Zou, S.; Schatz, G. C.; Van Duyne, R. P. Nanoscale Optical Biosensor: Short Range Distance Dependence of the Localized Surface Plasmon Resonance of Noble Metal Nanoparticles. *J. Phys. Chem. B* **2004**, *108*, 6961–6968.
19. Sherry, L. J.; Jin, R. C.; Mirkin, C. A.; Schatz, G. C.; Van Duyne, R. P. Localized Surface Plasmon Resonance Spectroscopy of Single Silver Triangular Nanoprisms. *Nano Lett.* **2006**, *6*, 2060–2065.
20. Sherry, L. J.; Chang, S. H.; Schatz, G. C.; Van Duyne, R. P.; Wiley, B. J.; Xia, Y. N. Localized Surface Plasmon Resonance Spectroscopy of Single Silver Nanocubes. *Nano Lett.* **2005**, *5*, 2034–2038.
21. Nehl, C. L.; Liao, H. W.; Hafner, J. H. Optical Properties of Star-Shaped Gold Nanoparticles. *Nano Lett.* **2006**, *6*, 683–688.
22. Sun, Y.; Xia, Y. Increased Sensitivity of Surface Plasmon Resonance of Gold Nanoshells Compared to That of Gold Solid Colloids in Response to Environmental Changes. *Anal. Chem.* **2002**, *74*, 5297–5305.
23. Wang, H.; Brandl, D. W.; Le, F.; Nordlander, P.; Halas, N. J. Nanorice: A Hybrid Plasmonic Nanostructure. *Nano Lett.* **2006**, *6*, 827–832.
24. Larsson, E. M.; Alegret, J.; Kall, M.; Sutherland, D. S. Sensing Characteristics of NIR Localized Surface Plasmon Resonances in Gold Nanorings for Application as Ultrasensitive Biosensors. *Nano Lett.* **2007**, *7*, 1256–1263.
25. Unger, A.; Kreiter, M. Analyzing the Performance of Plasmonic Resonators for Dielectric Sensing. *J. Phys. Chem. C* **2009**, *113*, 12243–12251.
26. Novo, C.; Funston, A. M.; Pastoriza-Santos, I.; Liz-Marzan, L. M.; Mulvaney, P. Influence of the Medium Refractive Index on the Optical Properties of Single Gold Triangular Prisms on a Substrate. *J. Phys. Chem. C* **2007**, *112*, 3–7.
27. Lee, J.; Hasan, W.; Odom, T. W. Tuning the Thickness and Orientation of Single Au Pyramids for Improved Refractive Index Sensitivities. *J. Phys. Chem. C* **2009**, *113*, 2205–2207.
28. Chen, H.; Kou, X.; Yang, Z.; Ni, W.; Wang, J. Shape- and Size-Dependent Refractive Index Sensitivity of Gold Nanoparticles. *Langmuir* **2008**, *24*, 5233–5237.
29. Khalavka, Y.; Becker, J.; Sonnichsen, C. Synthesis of Rod-Shaped Gold Nanorattles with Improved Plasmon Sensitivity and Catalytic Activity. *J. Am. Chem. Soc.* **2009**, *131*, 1871–1875.
30. Pastoriza-Santos, I.; Liz-Marzan, L. M. Synthesis of Silver Nanoprisms in DMF. *Nano Lett.* **2002**, *2*, 903–905.
31. Ledwith, D.; Aherne, D.; Kelly, J. M. Approaches to the Synthesis and Characterization of Spherical and Anisotropic Silver Nanomaterials. In *Metallic Nanomaterials*; Kumar, C. S. S. R., Ed.; Wiley-VCH: Weinheim, Germany, 2009; Vol. 1, p 99.
32. Kreibig, U.; Vollmer, M. *Optical Properties of Metal Clusters*; Springer: Berlin, 1995.
33. Voisin, C.; Del Fatti, N.; Christofilos, D.; Vallee, F. Ultrafast Electron Dynamics and Optical Nonlinearities in Metal Nanoparticles. *J. Phys. Chem. B* **2001**, *105*, 2264–2280.
34. Aherne, D.; Charles, D. E.; Brennan-Fournet, M. E.; Kelly, J. M.; Gun'ko, Y. K. Etching-Resistant Silver Nanoprisms by Epitaxial Deposition of a Protecting Layer of Gold at the Edges. *Langmuir* **2009**, *25*, 10165–10173.
35. Aherne, D.; Ledwith, D. M.; Gara, M.; Kelly, J. M. Optical Properties and Growth Aspects of Silver Nanoprisms Produced by a Highly Reproducible and Rapid Synthesis at Room Temperature. *Adv. Funct. Mater.* **2008**, *18*, 2005–2016.

36. Charles, D.; Fournet, P.; Cunningham, S.; Ledwith, D.; Kelly, J. M.; Blau, W.; Brennan- Fournet, M. E. A Sensitivity Study of the Localized Surface Plasmon Resonance of High Definition Structured Silver Nanoparticles in Solution. *Plasmonics: Metallic Nanostructures and Their Optical Properties Vi* **2008**, *7032*, G322.
37. Whelan, A. M.; Brennan, M. E.; Blau, W. J.; Kelly, J. M. Enhanced Third-Order Optical Nonlinearity of Silver Nanoparticles with a Tunable Surface Plasmon Resonance. *J. Nanosci. Nanotechnol.* **2004**, *4*, 66–68.
38. Yang, J.; Lu, L.; Wang, H.; Shi, W.; Zhang, H. Glycyl Glycine Templating Synthesis of Single-Crystal Silver Nanoplates. *Cryst. Growth Des.* **2006**, *6*, 2155–2158.
39. Liu, B.; Xie, J.; Lee, J. Y.; Ting, Y. P.; Chen, J. P. Optimization of High-Yield Biological Synthesis of Single-Crystalline Gold Nanoplates. *J. Phys. Chem. B* **2005**, *109*, 15256–15263.
40. Ding, Y.; Wang, Z. L. Structure Analysis of Nanowires and Nanobelts by Transmission Electron Microscopy. *J. Phys. Chem. B* **2004**, *108*, 12280–12291.
41. Kulkarni, A. P.; Munechika, K.; Noone, K. M.; Smith, J. M.; Ginger, D. S. Phase Transfer of Large Anisotropic Plasmon Resonant Silver Nanoparticles from Aqueous to Organic Solution. *Langmuir* **2009**, *25*, 7932–7939.
42. Malinsky, M. D.; Kelly, K. L.; Schatz, G. C.; Van Duyne, R. P. Chain Length Dependence and Sensing Capabilities of the Localized Surface Plasmon Resonance of Silver Nanoparticles Chemically Modified with Alkanethiol Self-Assembled Monolayers. *J. Am. Chem. Soc.* **2001**, *123*, 1471–1482.
43. Miller, M. M.; Lazarides, A. A. Sensitivity of Metal Nanoparticle Surface Plasmon Resonance to the Dielectric Environment. *J. Phys. Chem. B* **2005**, *109*, 21556–21565.
44. Svedendahl, M.; Chen, S.; Dmitriev, A.; Kall, M. Refractometric Sensing Using Propagating *versus* Localized Surface Plasmons: A Direct Comparison. *Nano Lett.* **2009**, *9*, 4428−4433.
45. Zhu, S.; Li, F.; Du, C.; Fu, Y. A Localized Surface Plasmon Resonance Nanosensor Based on Rhombic Ag Nanoparticle Array. *Sens. Actuators, B* **2008**, *134*, 193–198.
46. Mie, G. Contributions to the Optics of Turbid Media Particularly of Colloidal Metal Solutions. *Ann. Phys.* **1908**, *25*, 377.
47. Palik, E. D. *Handbook of Optical Constants of Solids*; Academic Press, Inc: New York, 1985.
48. Link, S.; El-Sayed, M. A. Spectral Properties and Relaxation Dynamics of Surface Plasmon Electronic Oscillations in Gold and Silver Nanodots and Nanorods. *J. Phys. Chem. B* **1999**, *103*, 8410–8426.
49. Haes, A. J.; Van Duyne, R. P. A Unified View of Propagating and Localized Surface Plasmon Resonance Biosensors. *Anal. Bioanal.Chem.* **2004**, *379*, 920–930.
50. Draine, B. T.; Flatau, P. J. Discrete-Dipole Approximation for Scattering Calculations. *J. Opt. Soc. Am. A* **1994**, *11*, 1491–1499.
51. Jin, R.; Cao, Y.; Mirkin, C. A.; Kelly, K. L.; Schatz, G. C.; Zheng, J. G. Photoinduced Conversion of Silver Nanospheres to Nanoprisms. *Science* **2001**, *294*, 1901–1903.